International Journal of Environmental Sciences
ISSN: 2229-7359
Vol. 11 No. 21s, 2025
https://www.theaspd.com/ijes.php

M-BTC (M = Ga, Zr, Al, Cu) MOFs For The Efficient Removal Of Toxic Heavy Metal Ions From Water: Synthesis, Characterization And Adsorption Studies

Swaroopa Chilkamarri[1], Vennela Aluvala[1], Venkatesham Kothabai[1], Vijayalaxmi Burri[1], Vijayatha Myadam[1], Venkataswamy Perala[1], Sasikumar Boggala[2], Anjaneyulu Chatla[2], Ramaswamy Kadari[3], Hari Padmasri Aytam[1*]

[1]Department of Chemistry, University College of Science, Osmania University, Hyderabad 500 007, Telangana, India.
[2]Catalysis and Fine Chemicals Department, CSIR - Indian Institute of Chemical Technology, Hyderabad-500 007, Telangana, India.
[3]ROHS laboratory, Centre for Materials for Electronics Technology, Cherlapally HCL (PO), Hyderabad - 500051, Telangana, India.
*Correspondence author: Email ID : ahpadmasri@osmania.ac.in; ahpadmasri@gmail.com

Abstract: *Simple 1,3,5-benzene tricarboxylic acid (BTC) linkaged metal organic frameworks (MOFs) with four different metal nodes namely Ga, Zr, Al and Cu were prepared by solvo-hydrothermal technique. These BTC MOFs were well characterized by adsorption-spectroscopic techniques to establish their structural, morphological and chemical characteristics. The unique and advantageous properties of MOFs such as micro crystallinity, microporosity and high surface area were responsible for their high adsorptive capacities in the removal of toxic heavy metal ions from aqueous solutions. Among the four different MOFs studied Ga-BTC MOF was recognized as a high potential and selective material for removal of heavy metal ions over the rest of the MOFs. It displayed greater selectivity for the adsorption of Pb2+ions with a maximum adsorption capacity of 976 mg g-1 even without any specific N or S containing functional groups or magnetic component. The adsorption studies were carried out by estimating the amounts of heavy metal ions adsorbed by ICPOES analysis and confirmed from SEM-EDX data. It further exhibited reusability for 5 cycles with its structure remaining intact as observed from the XRD patterns.*
Keywords: *BTC, MOF, heavy metal ion, adsorption, ICPOES, SEM-EDX.*

INTRODUCTION

Environmental degradation is a major global concern today resulting in the decline in the quality of natural environmental elements primarily air, soil and water which in turn is detrimental affecting the natural habitat in terms of the health, well-being and even responsible for the extinction of certain species. Mankind is extremely impacted by high pollutant concentrations viz., volatile organic pollutants, heavy metal ions and the plastic waste from human activity majorly from industries, creating havoc in terms cancerous and many other diseases that affect the metabolism and quality of life in humans. Heavy metal ions are non-biodegradable and have high adsorption capacity in biological systems, hence can easily penetrate into the food chain through the marine life. The concentrations of these ions beyond 5 g/cc itself are considered as toxic but many industrial effluents can have concentrations of these ions as high as ppm [1]. The heavy metal ions beyond this limit can cause high risk health hazards such as cancer, organ damage, obstructing the development and growth, destruction of nervous system, kidneys and brain, causing various autoimmune diseases such as rheumatoid arthritis as well [2]. Industries dealing with alloys, ceramics, plastics, glassware, lead-acid batteries, antiknock agents etc., are in general the main sources from where lead comes out as one of the major pollutants in the effluent streams[3]. While anthropogenic sources of mercury are the metal extraction processes, Hg vapor lamps, electrical equipment, dental filling, scientific instruments and pharmaceuticals[4]. Excess of lead in water/oil can be highly fatal. While excess amounts of mercury can cause minamata disease, intestinal disorders, urinary problems, paralysis etc. [5]. The common sources of Cd are known to be from mining, refining, food and fertilizers [6]. Cadmium in excess amounts cause health problems such as itai-itai disease, neurodegenerative disorders and cancers [7]. They also contaminate the environment by various means such as causing soil, air and water pollution destroying both flora and fauna. These heavy metal ions can reach to the bottom of the food chain causing high levels of toxicity in fish and other sea foods too Toxic metal

ions may be removed from environmentally polluted matrices by various physico-chemical methods such as ion-exchange, precipitation, ultrafiltration using membranes and adsorption [8]. Among these methods reported, adsorption is a preferable and efficient method [9] due to the ease of operation, small quantities of materials used that can remove large quantities of heavy metal ions over adsorbents of high surface area and porosity that are highly efficient in the removal of toxic metal ions. Several carbonaceous, silica based, metal oxides, polymers, clays and zeolitic materials have been explored in this regard [10-12]. MOFs are versatile, robust and highly tunable materials that exhibit possess high surface area, porosity and metal ion nodes and organic linkers that are also selective in adsorbing the toxic metal ions through electrostatic and other non-covalent interactions[13-16].

MOFs are known to exhibit exceptional adsorption properties mainly by four different means viz., surface adsorption, pore infiltration, adsorption through covalent interactions and encapsulation adsorption of molecules [17]. The metal ion nodes that act as coordinately unsaturated sites as well as the functional groups of the organic linkers are the main target sites for the adsorbates. The potential of MOFs as adsorbents depends on the coordination ability of metal ion and interactions of organic linkers with the adsorbates [18]. Several MOFs were reported as potential adsorbents for the removal of toxic heavy metal ions and further that are either functionalized in general with N or S containing ligands [19, 20] or composites of MOFs with magnetic materials such as Fe_3O_4 exhibited much higher adsorption capacities of heavy metal ions [21, 22]. MOFs viz., UiO-66-NH_2[23], TMU-31 [24], thiazole functionalized Zn-MOF [25], Zr-MOF [26] are reported to show high removal efficiency of Pb(II) ions from aqueous medium. While nFe_3O_4@MIL-88A(Fe) [27] and TMU-5 [28] were very selective in adsorbing Cd(II) ions. Hg(II) ions were reported to have been removed efficiently by Fe_3O_4 - JUC-62 [29], thiazole functionalized Zn-MOF [25], UiO-66-NHC(S) [30], thiol-Cu-BDC MOF [31] and TMU-31[24]. The present report is a study of toxic heavy metal ions removal from aqueous solutions using simple BTC based MOFs. Influence of various parameters such as pH, contact time and concentration of the metal ions on the removal efficiency of MOFs were also studied in detail for exploring the maximum adsorption capacities of MOFs under study.

EXPERIMENTAL DETAILS

Materials used

All the chemicals used in this study were of Sigma-Aldrich (India) make and were used as supplied without any further purification. The chemicals used are gallium nitrate trihydrate, copper nitrate trihydrate, zirconium chloride, aluminium nitrate nona hydrate, N,N-dimethyl formamide, ethanol, methanol, acetone, acetic acid and 1,3,5-benzene tricarboxylic acid (BTC).

Synthesis of MOFs

Cu-BTC MOF is prepared [32] using benzene-1, 3, 5-tricorboxylic acid (4.91 g, 0.0234 mol) dissolved into ethanol and DMF mixture (1:1) (25mL) and Cu $(NO_3)_2$.$3H_2O$ (10.86g, 0.0466 mol) was dissolved into water (25mL). The two solutions were mixed at ambient temperature for 30 min, and transferred into an auto clave heated at 85℃, under hydrothermal conditions for 24 h. The blue crystals obtained after cooling the autoclave were isolated by decanting the mother liquor, washed with DMF. Ethanol was used for solvent exchange followed by drying the product under vacuum for 6h at 170 ℃. The Cu-BTC MOF in the final form was obtained as deep purple crystals. While the Ga-BTC MOF, was synthesized [22] from a mixture of Ga $(NO_3)_2$.$6H_2O$ (0.4172 g) and BTC (0.2522 g) in 12 mL DMF. The reactants were magnetically stirred and heated for 10 h at 100 °C. The mixture was cooled to the room temperature .The mixture was centrifuged (8000 rpm, 5 min) and the obtained white precipitate was washed with DMF three times.

Zr-BTC was obtained [33] by dissolving 0.1165 g (0.50 mmol) of $ZrCl_4$ and 0.0353 g (0.168mmol) of 1,3,5-benzenetricarboylic acid in 2.8 ml of acetic acid and 5 ml of N,N-dimethylformamide. The mixture was stirred for 15 minutes at ambient temperature before subjecting it to hydrothermal treatment at 120℃ for 24 hours. The cooled mixture was filtered, washed with DMF, acetone and methanol and finally activated at 200℃ for 2 hours. Al-BTC MOF was synthesized by the solvothermal method [34] using a precursor of aluminium nitrate nano hydrate (0.047 g, 2 mmol) and BTC (0.630 g, 3 mmol) in DMF (30 mL) kept without stirring at 130 °C for 72 h in a Teflon-lined autoclave. The autoclave was then cooled to ambient temperature, and the solid obtained was separated by centrifuging it at 6000 RPM for 5 min. Then it was washed with DMF under sonication for 10 min, followed by

washing with methanol at ambient temperature. Further it was washed with hot (70 °C) methanol for 5 h and dried under vacuum at 80 °C overnight.

Characterization of MOFs

All the as synthesized MOFs were investigated by various techniques viz., XRD, sorption studies, UV-DRS, FT-IR, DTA/TG, PL, SEM-EDX and XPS. X-ray diffractograms were recorded on a Rigaku Miniplex X-ray diffractometer with an X-ray source as Ni filtered Cu Kα radiation (λ = 0.15418 nm) and the samples were scanned at a speed of 2° min^{-1} and from scan 5-80° at 40 kV and 20 mA. While the sorption studies were carried out a Micromeritics ASAP 2010 instrument at liquid nitrogen temperature and the surface areas were evaluated using BET-equation and also pore size and pore volume of the MOFs were also derived from the sorption studies. A Perkin Elmer STA 6000 Instrument was employed for recording TGA curves from room temperature to 800 °C at the rate of 20 °C min^{-1} in nitrogen flow. UV–Vis diffuse reflectance spectra (UV DRS) were obtained on a JASCO V650 UV–Visible spectrophotometer in the wavelength range of 200–800 nm equipped with a dual D2/W lamp for UV-visible range recording and a photomultiplier R357U tube with a metal alkali photocathode detector. SEM -EDS data were recorded using JEOL, JSM—6390LV and Oxford XMX N instrument. A Thermo Nicolet iS50 with inbuilt ATR, Thermo Fisher Scientific instrument was used for FT-IR spectra of all the samples by KBR pellet method. XPS analysis of all the MOFs was carried using Mg K_α radiation on a KRATOS-AXIS 165 instrument.

Adsorption of heavy metal ions over MOFs

Removal of heavy metal ions viz., Pb^{3+}, Hg^{2+} and Cd^{2+} from aqueous matrix was studied by preparing their respective salt solutions of different concentrations (mg/L). About 50 mL of these solutions individually were taken in batches and ~10mg of each MOF was soaked separately and stirred on a magnetic stirrer at room temperature. The samples at different time intervals were collected and submitted for ICPOES analysis. The solution was filtered to remove the MOF material which was then dried in an oven and submitted for SEM-EDAX analysis. The ICPOES analysis gave the remaining amount of heavy metal ions present in the solution while the EDAX analysis showed the actual amount of heavy metal ion adsorbed on the surface of MOF. The tests were conducted for four different BTC based MOFs synthesized and characterized. Effect of pH was studied at different pH conditions for maximum adsorption of metal ions over MOF materials. The %removal efficiency of the heavy metal ions was calculated using the equation:

% removal efficiency = $\frac{C_0 - C_t}{C_0}$ x 100 where C_0 is the initial concentration of the heavy metal ions taken before adsorption and C_t is the remaining concentration of the heavy metal ions after adsorption at time 't'.

RESULTS AND DISCUSSION

Powder X-ray diffraction analysis

Figure 1 represents the powder X-ray diffractograms of the four different BTC linkage MOFs synthesized. All the BTC MOFs showed distinguished diffraction peaks in the range of 10-30° that are characteristic of MOFs [35]. Ga-MOF showed the diffraction lines specifically that correspond to the orthorhombic crystal structure [36] while Cu-MOF exhibited peaks corresponding to FCC structure with the MOF phase that matched with JCPDS no. 00-062-1183 [37]. Al BTC peaks were observed at 6.7°, 10.3°, 11.6°, 13.5°, 14.7°, 19.3°, 25.9° and 28.9° that are assigned to the (200), (220), (222), (400), (331), (440), (731), and (751) miller planes respectively (ICDD#00-062-1183 [35]. Two prominent peaks observed in case of cubic crystalline Zr BTC MOF were at 8.32° and 8.69° ascribed to the (311) and (222) planes [38]. There was a shift in the main diffraction peaks from Cu-MOF to Zr-MOF and the extent to which the peaks shifted was in the increasing order of atomic radii from Cu^{2+} to Zr^{4+} [35]. The structural disorder was greater with the increase the atomic radii of the metal ions. However, all the MOFs have shown high crystallinity, with the crystallite size nearly the same in nano range (table 1).

International Journal of Environmental Sciences
ISSN: 2229-7359
Vol. 11 No. 21s, 2025
https://www.theaspd.com/ijes.php

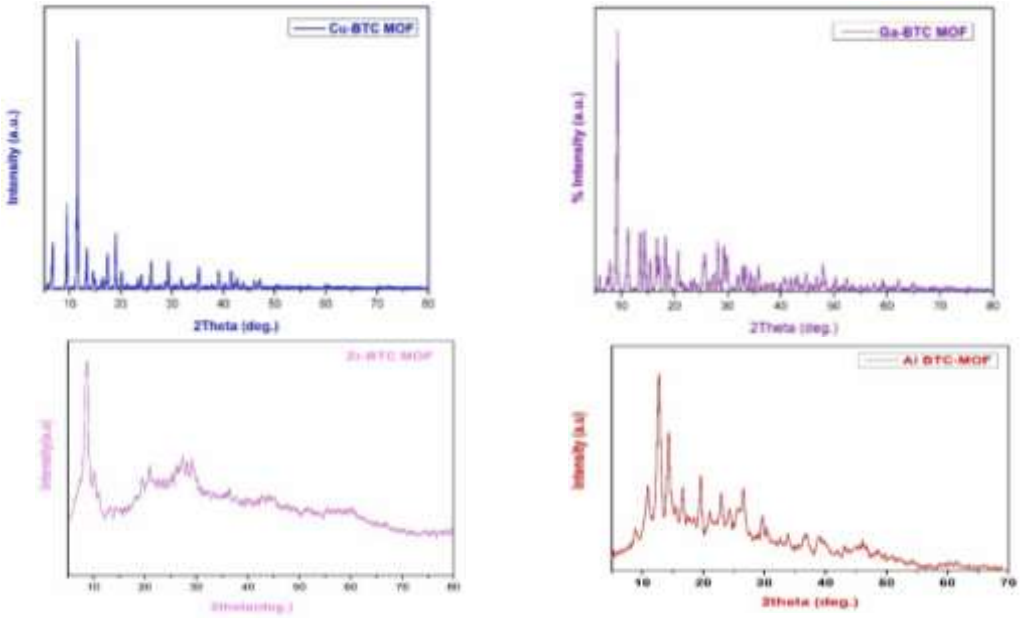

Figure 1: XRD patterns of the MOFs

Table-1: Crystallographic and structural characteristics of MOFs

MOFs	BET-SA (m^2g^{-1})	Average Pore radius (nm)	Pore volume (cc/g)	Crystallite Size (nm) from XRD
Cu-BTC	1099	0.89	0.56	13.1
Ga-BTC	1017	0.62	0.46	12.4
Al-BTC	1321	0.82	0.59	11.9
Zr-BTC	902	0.97	0.94	13.3

N_2 Sorption studies

All the four BTC MOFs showed a type-1 adsorption isotherm (as per IUPAC) (fig. 2). The MOFs are microporous in nature as can be deduced from the type of adsorption isotherm and a sudden rise in adsorption above P/P_0 of 0.05 itself. They exhibited high specific surface areas as presented in table 1. However, they also possess certain amount of mesopores as well. Al MOF showed higher surface area owing it to the presence of certain mesopores indicating greater thermal stability of this MOF [39]. The pore radii of the MOFs were found to be in the range of 0.6-1.0 nm. Ga MOF exhibited the narrower pores among all the other MOFs studied. These MOFs had certain portion of mesopores as well with Al MOF containing more mesopores than the rest three M-MOFs.

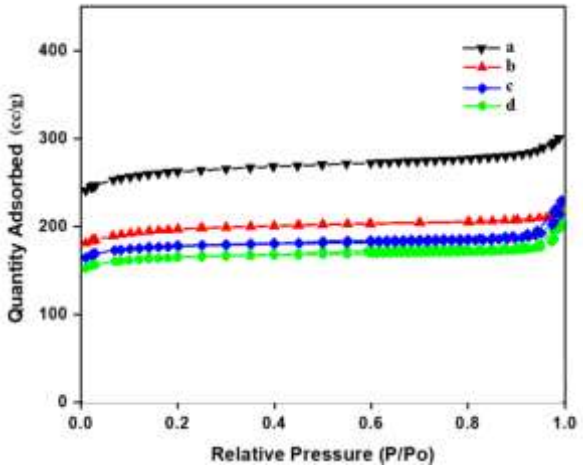

Figure 2: N_2 sorption isotherms of a) Ga b) Zr c) Al d) Cu MOFs

Thermogravimetric analysis

The thermogravimetric profiles of MOFs in general are reported and observed to undergo three transitions of weight loss:

i). First stage of weight loss is due to the physisorbed water molecules, the percentage of which varied with type of MOF both in terms of the metal ion and organic linker.

ii). A second stage loss was corresponding to the trapped up solvent species which also was different from metal to metal and ligands present in the MOF.

iii). The last stage of weight loss the corresponding temperature is indicative of the stability of the MOF where in the organic linkers start decomposing and leaving the structure to deform.

Upon further heating beyond this stage a burial of MOF could be seen with final transformation to its corresponding metal oxide.

All the MOFs under current study are BTC ligand based and hence have similar patterns of TG curves (fig. 3) yet each varied in terms of the shape of the curves as temperature range and extent of weight loss differed from one another with the different metal ions of MOFs studied viz., Ga^{3+}, Zr^{4+}, Al^{3+} and Cu^{2+}.

In the TG pattern of Ga MOF, the first weight loss occurred from RT upto 50 °C that was attributed to about 2.2 water molecules per metal ion associated with the MOF [36].The second stage of loss in weight at 50-150 °C was reported as to the loss of 0.8 DMF molecules per a metal unit accounted for about 17.4% of total weight loss. And the final loss was about 43.3% with the decomposition of the BTC ligand from 400 °C above which the structure collapses to form its oxide, Ga_2O_3.

A 26.5% loss of mass due to the release surface adsorbed water and solvent molecules below 300 °C in case of Zr MOF [40]. A further heating led to a loss of 43% of weight in the range of 450-600°C ascribed to the breakdown of the organic linker, trimesic acid.

The characteristic features observed in case of Al MOF are the two stages of weight loss at 270–320 °C and 500–650 °C respectively corresponding to the solvent molecules adsorbed in the pores and disintegration of the MOF network structure with the BTC linker decomposition [41]. This profile indicates the high thermal stability of Al MOF over other M MOFs studied here. Cu-BTC MOF exhibited a first stage weight loss ~8% owing to the loss of physisorbed water and solvent molecules while the second corresponding to a loss of 20% in the temperature range of 200-350 °C and the last stage weight loss of 9% above 320 °C due to the loss of organic linker molecules and the decomposition of the MOF material respectively. [42].

International Journal of Environmental Sciences
ISSN: 2229-7359
Vol. 11 No. 21s, 2025
https://www.theaspd.com/ijes.php

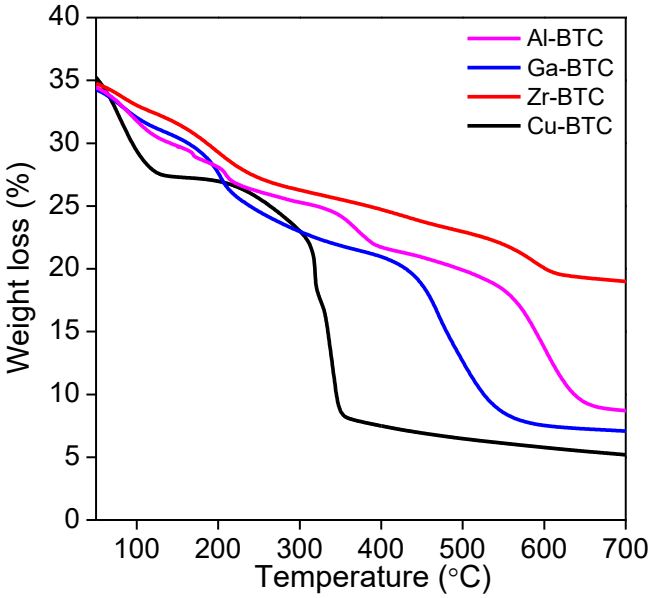

Figure 3: TG Curves of MOFs

3.4. SEM-EDX Results

All the MOFs as synthesized showed polyhedron morphology with some variations in the size and shape of the particles in general. The morphology of Ga-BTC particles was of octahedral and dodecahedral shaped with an average particle size ≤ 10 μm. While the particles of Zr BTC were more defined and of octahedral morphology whose size ranged below 10 μm. The Cu-& BTC crystals form cubo-octahedral and trapezoidal structures with Al MOF whose particles being more uniform and definite while Cu MOF particles were of variable lengths, width and size of faces as noticed from the SEM images (fig.4). The images indicate MOF particle size in between 5-10 μm. EDX results (fig.4) confirm the elemental composition of the MOFs and the composition in wt.% is presented in the inset figures of EDX spectra of the MOFs.

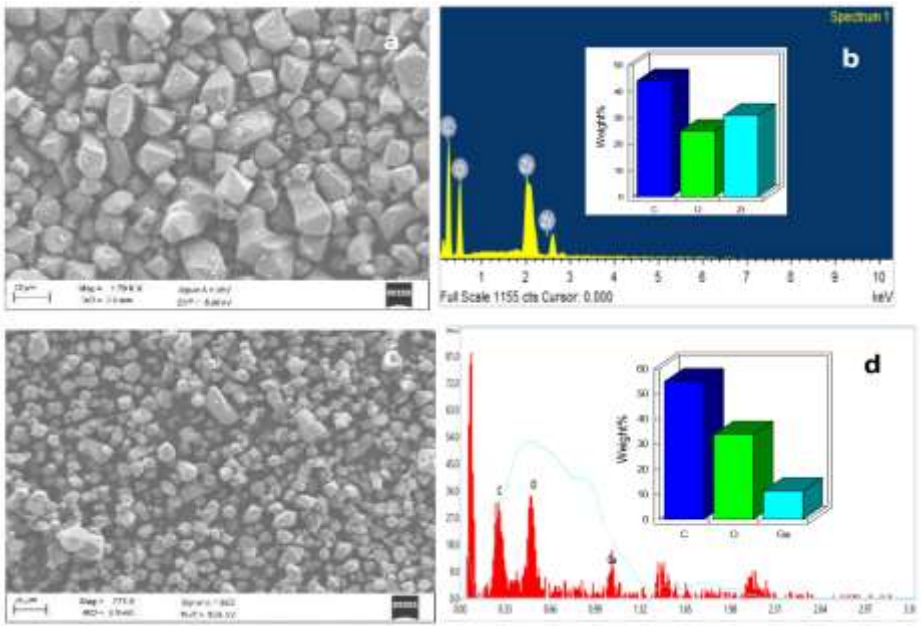

International Journal of Environmental Sciences
ISSN: 2229-7359
Vol. 11 No. 21s, 2025
https://www.theaspd.com/ijes.php

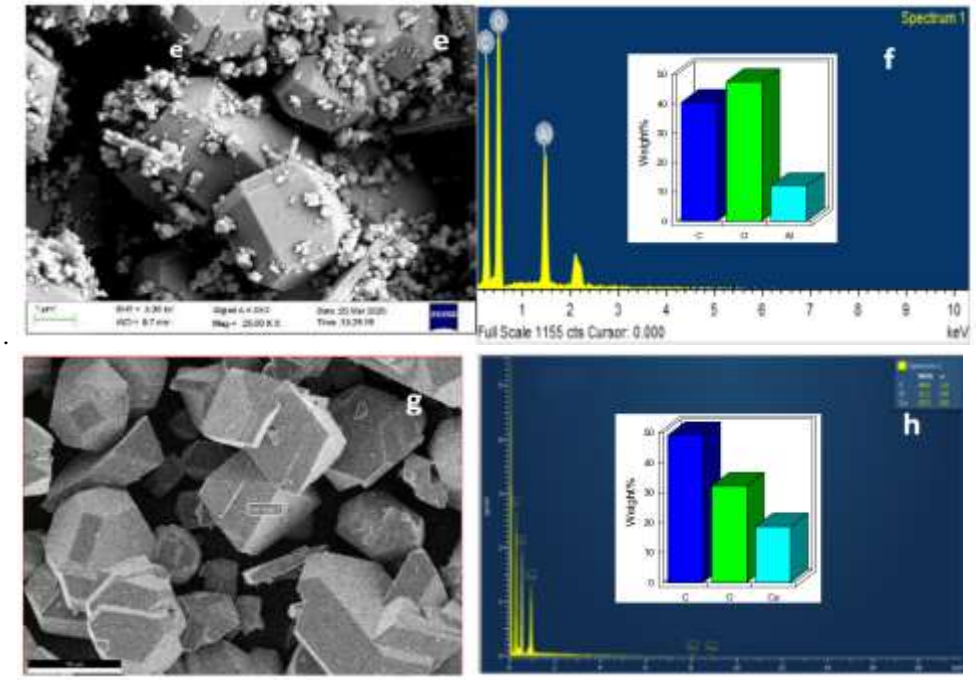

Figure 4: SEM-EDAX images of MOFs - a) &b) Ga; c) & d) Zr;

e) & f) Al; g) & h) Cu

3.5 FT-IR analysis

The IR spectrum of Al MOF (fig.5) showed bands at 1574 and 1505 cm^{-1} due to the symmetric stretching of -COO group of BTC linkers while the asymmetric ones appear at 1443 and 1397 cm^{-1} [38]. The stretching bands of free BTC inside the pores are reported in the range 1730-1650 cm^{-1} that disappear on activation. The bending and stretching modes of bridging hydroxyl groups are further shown to have appeared at 1630 and 3607 cm^{-1} respectively [43]. Zr BTC MOF showed vibrational modes ~650 cm^{-1} and 757 cm^{-1} of Zr-O indicating a strong coordination of carboxylic acid group of the trimesic acid with the Zr ion [44]. Further, the characteristic peak of -COOH group of BTC ~1700 cm^{-1} which was attributed to the physisorbed carboxylic acid group in the framework. The rest of the pattern showed signals similar to the rest of MOFs corresponding to the presence of organic linker BTC. Ga-BTC IR spectra was similar to the rest of the MOFs pertaining to the frequencies of vibrations of the benzene-1,3,5-tricarboxylic acid linker that is common to all the M-MOFs in the study. The IR spectrum of Cu-BTC exhibited vibrational bands at 480 and 720 cm^{-1} corresponding to the stretching and bending modes of Cu–O are observed (fig. 5) while the characteristic bands of BTC were observed from 800–1150 cm^{-1} assigned to the stretching modes of O–C=O and C–O with the bending modes in between 660–760 cm^{-1}. Strong Peaks at 1375, 1432 and 1625 cm^{-1} also correspond to the carboxylic group of the BTC linker [45]

International Journal of Environmental Sciences
ISSN: 2229-7359
Vol. 11 No. 21s, 2025
https://www.theaspd.com/ijes.php

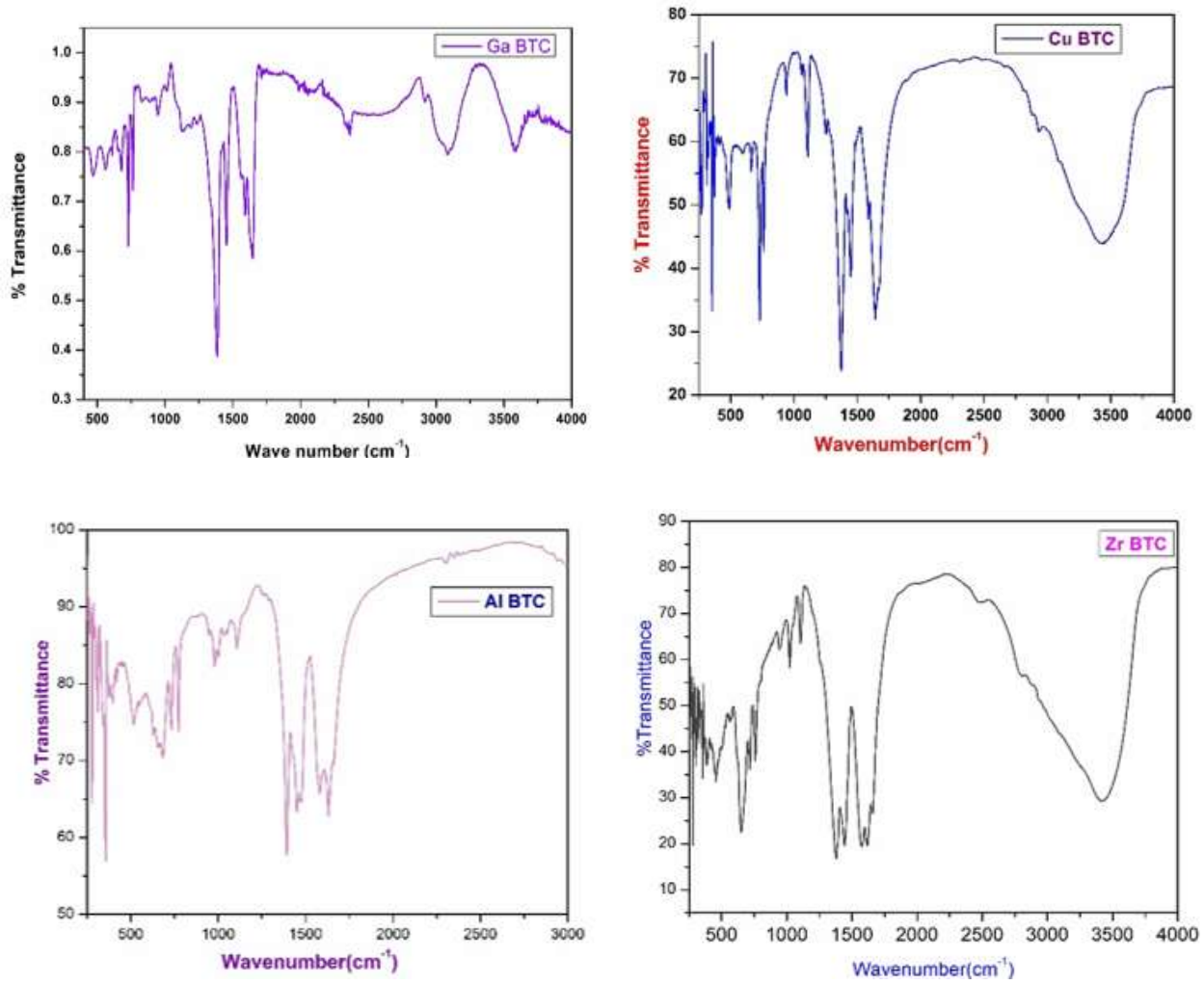

Figure 5: FT-IR spectra of MOFs

3.6. Raman Spectral Data analysis

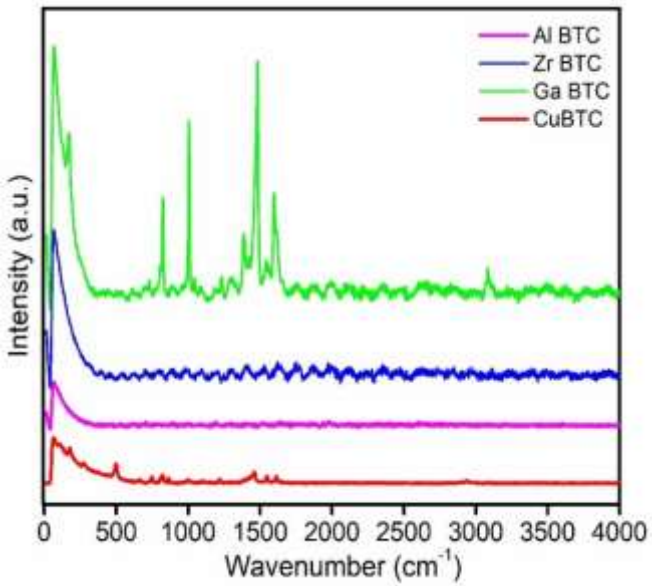

Figure 6: Raman spectra of MOFs

In the Raman spectra of fig. 6, the modes of vibration of C=C in the benzene ring of the BTC linker were seen as a strong and intense band at 1100 cm^{-1} and a weak band ~1500 cm^{-1} [46]. Apart from these a band at 780 cm^{-1} was also noted corresponding to the out of plane C-H bending vibration of the aromatic ring. Broad bands were obtained in between 300-400 cm^{-1} which were reported to be associated with metal-O stretching vibrations. Further the presence of D-and G-bands ascribed to disordered structure and to the vibrations sp^2 carbon atoms of the organic linker, BTC of the MOF [46, 47]. A peak around 210 cm^{-1} was ascribed to the Raman mode of Ga-O indicating the presence and interaction of Ga^{3+} with the organic linker, BTC [48]. The other characteristic vibrations of the ligand BTC that was described in case of Ga BTC MOF are of low intensity in the spectrum. While the Al MOF showed the generally observed Raman modes of the BTC as discussed above seen as low intensity peaks in this spectrum. A broad peak in the range of 200-300 cm^{-1} probably suggests the linkage of Al^{3+} with the terephthalic acid linker in the MOF. A similar conclusion can be made from the Zr MOF Raman spectra which only exhibited a broad peak in between 200-300 cm^{-1}. The characteristic Cu-O and Cu-Cu peaks were observed in the range of 200-270 cm^{-1} in case of Cu BTC MOF. While a low intensity peak at 450 cm^{-1} could be ascribed to the vibrational stretching modes of Cu-O . The C-H bending modes of the phenyl group of the organic linker can be seen ~600-1200 cm^{-1} [49].

3.7. UV-DRS analysis

A technique used to analyze the optical properties of solid and powdered samples by measuring how much light they reflect across the ultraviolet and visible wavelengths. UV-DRS measure the diffuse reflectance of a sample as a function of wavelength. UV-DRS is useful for studying the electronic structure, band gap energy of crystals. The absorption bands (fig. 7) can be observed between 200-300 nm for Zr BTC MOF while Al BTC, Ga BTC and Cu BTC show from 200-600 and 200-800 nm respectively. The absorption bands between 200-300 nm corresponds to the π—π* and n- π* transitions exhibited by ligand BTC and due to Ligand to Metal Charge Transfer (LMCT) [50]. The extended absorption around 700 nm in case of Cu-BTC MOF is due to the d-d transitions of the Cu^{2+} ions. Ga and Al-MOFs also exhibited a broad absorption band beyond 400 nm upto 600 nm.

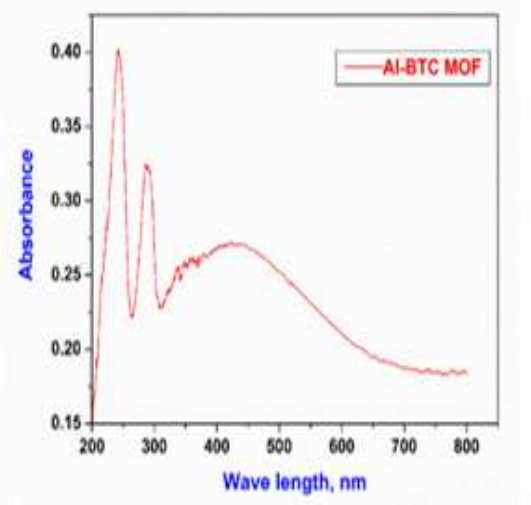

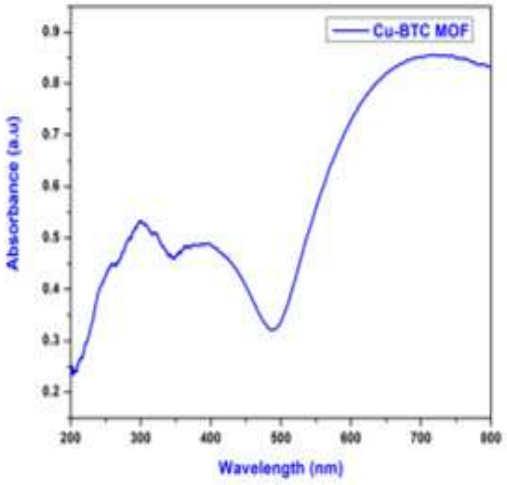

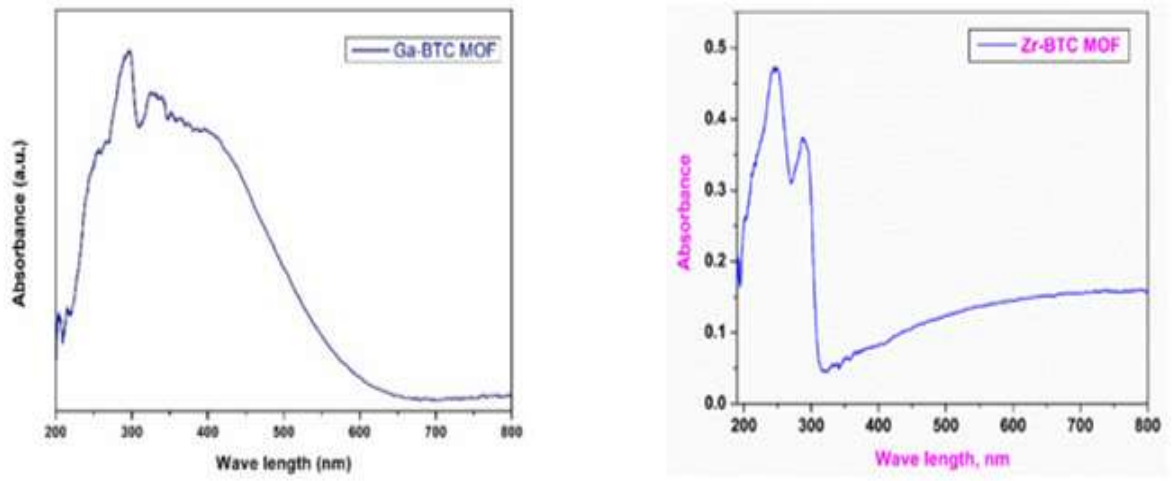

Figure 7: UV-DRS spectra of MOFs

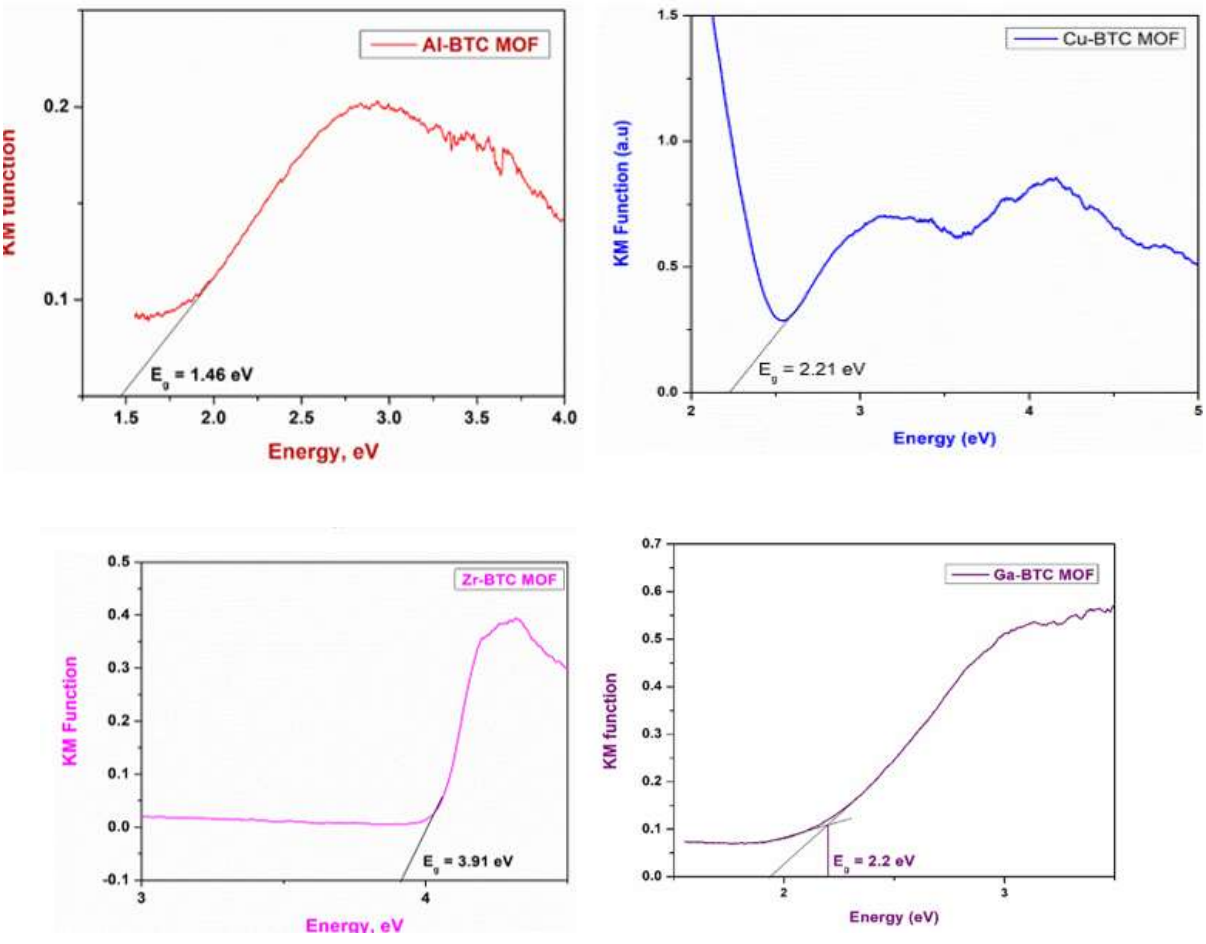

Figure 8: UV-DRS Tauc Plots of MOFs

The Kubelka-Munk equation was applied to estimate the bandgap energy (E_g) of MOFs:
$(\alpha h\nu)^2 = A(h\nu-E_g)^{n/2}$
where α, h, υ, and A are the diffuse absorption coefficient, Planck's constant, light frequency, and constant,

respectively.

It may also be obtained by $\mathbf{E_g = \frac{1240}{\lambda}}$

The bandgap values from figure 8 and absorption wavelengths indicate that Zr BTC MOF has greater absorption in UV region while Al, Ga and Cu BTC MOFs showed shift in their absorption wavelengths extended to visible region as indicated by their bandgaps as well.

3.8. XPS Results

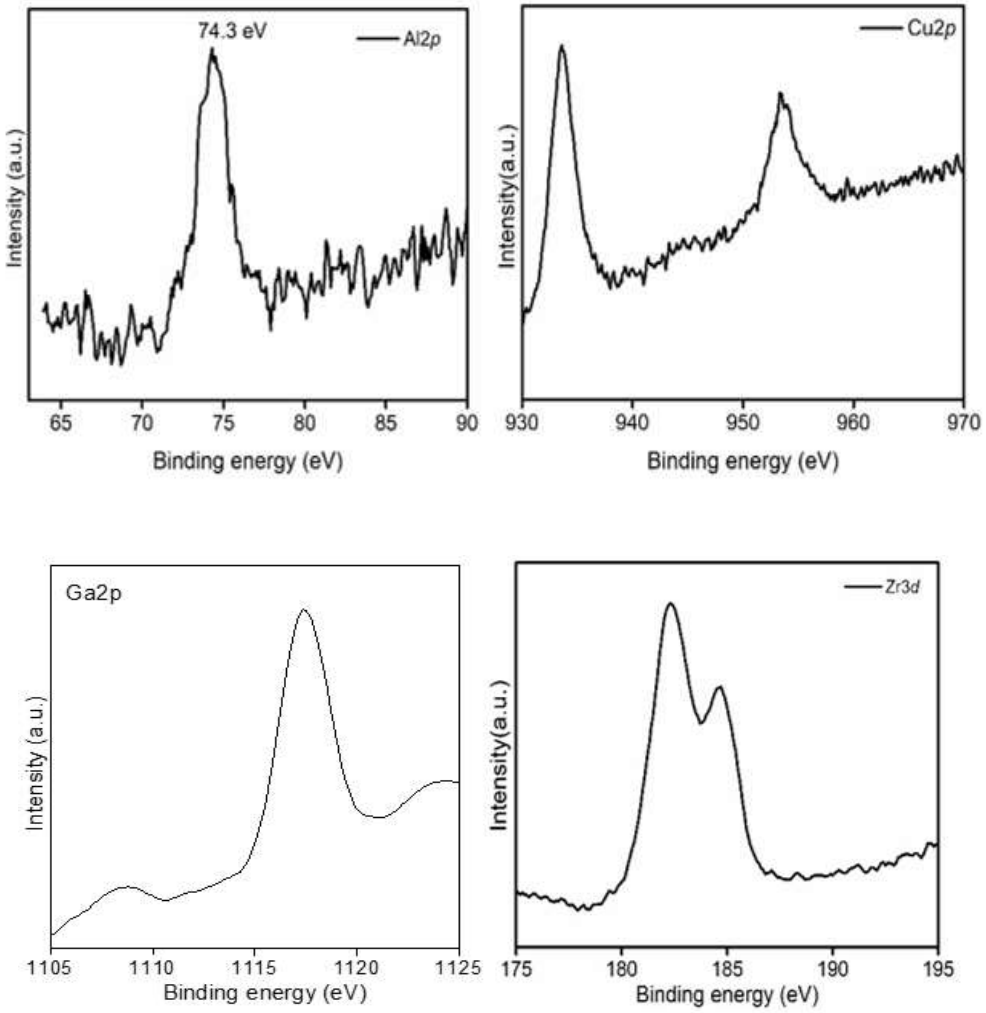

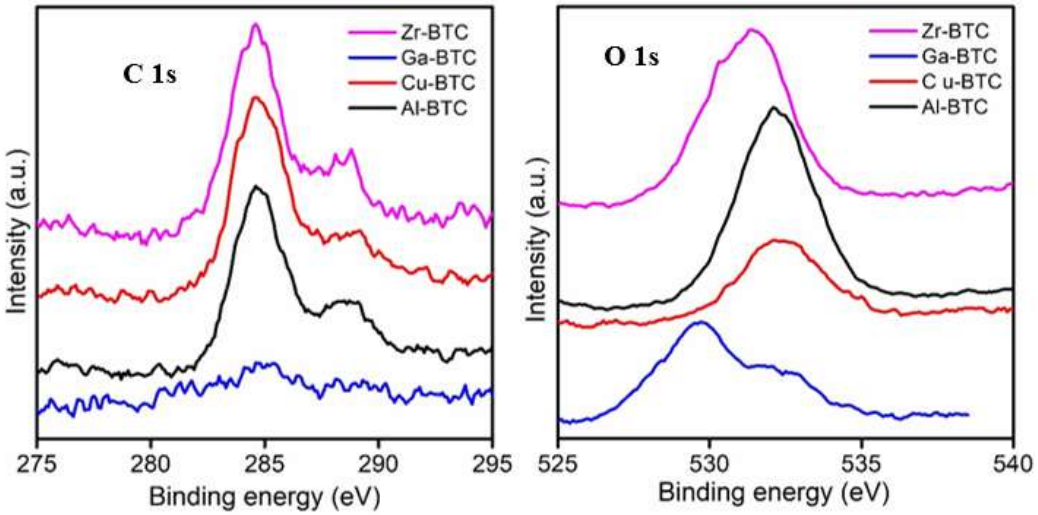

Figure 9: XPS spectra of Al 2p, Cu 2p, Ga 2p, Zr 3d, C1s and O1s of the MOFs

Figure 9 represents the XPS spectra of the various elements present on the surface of the MOFs under study. Al 2p peak was obtained at a B.E. of 75 eV suggesting the Al^{3+} state of the element in Al MOF [51]. Zr 3d is split into Zr $3d_{5/2}$ and Zr $3d_{3/2}$ appearing at ~182 and 185 eV respectively separated by nearly 3 eV indicative of Zr-O and Zr interacted to carboxylate group [52]. While Ga 2p peak can be seen at a B.E. of 1117 eV which shows Ga^{3+} presence in Ga MOF [53]. The O 1s of all these MOFs showed a broad peak which may be deconvoluted to eV attributed to O^{2-} in the crystal structure of the MOFs [54]. This peak shifted to slightly higher B.E. in case of Ga MOF. Cu $2p_{1/2}$ and Cu $2p_{3/2}$ signals were observed at 935.5 and 955.3 eV (fig. 8) which are due to Cu(II) in Cu BTC MOF which further exhibited two satellite peaks at ~ 964.5 eV and ~942 & ~945 eV respectively [55]. The other signals at ~933.5 and ~954 eV are attributed to Cu $2p_{3/2}$ and Cu $2p_{1/2}$ in Cu(I) form.

Adsorptive removal of toxic heavy metal ions by MOFs

Batch Adsorption studies

Toxic heavy metal ions viz., Pb^{2+}, Hg^{2+}, Cd^{2+}, Sn^{4+} and Sb^{5+} removal from aqueous solutions of their respective salts (section 2.1) was studied over the MOFs synthesized. Different concentrations of the heavy metal ion solutions (in ppm) were prepared in this regard. MOFs having a high surface area, are highly potential adsorbents that can remove high concentrations of the toxic heavy metal ions. Adsorption of heavy metal ions is both by means of physical as well as chemisorption over MOFs materials which is another added advantage as efficient material for the removal of these metal ions. Adsorption process is dependent on factors such as temperature, pH, contact time, concentration the adsorbates and nature of adsorbents viz., amount, surface area and particle size taken.

Effect of pH on the removal efficiency of heavy metal ions over MOFs

In the present study firstly, Ga BTC MOF prepared was tested for adsorption of lead ions at different concentrations in the range of 20-400 ppm at an optimized pH of 5. pH optimization was done over Ga BTC MOF at different pH conditions ranging from 1-7. A maximum adsorption was observed at pH 5 (fig. 10) when 20 ppm of Pb^{2+} solution was tested over Ga BTC MOF, thus it was chosen as the optimum pH condition for rest of the studies carried out in this work. pH affects the adsorption efficiency greatly. It was observed that low pH (high acidic)/high pH (high basic) condition is not favorable for the adsorption of lead ions. It is reported [56] that the pH should be greater than the isoelectric point of MOF which results in a net negative charge on MOF that enhances the electrostatic interaction between the surface metal nodes of MOF with the heavy metal ions and thus in their increased adsorption capacity of heavy metal ions. At lower pH the H_3O^+ can compete with the heavy metal ions thus lowering their adsorption capacity while at higher pH, the adsorption can be lowered with a possible precipitation of the heavy metal ions as hydroxides [57]. Thus, pH 5 is chosen as optimum condition for the heavy metal ions removal over the MOFs.

International Journal of Environmental Sciences
ISSN: 2229-7359
Vol. 11 No. 21s, 2025
https://www.theaspd.com/ijes.php

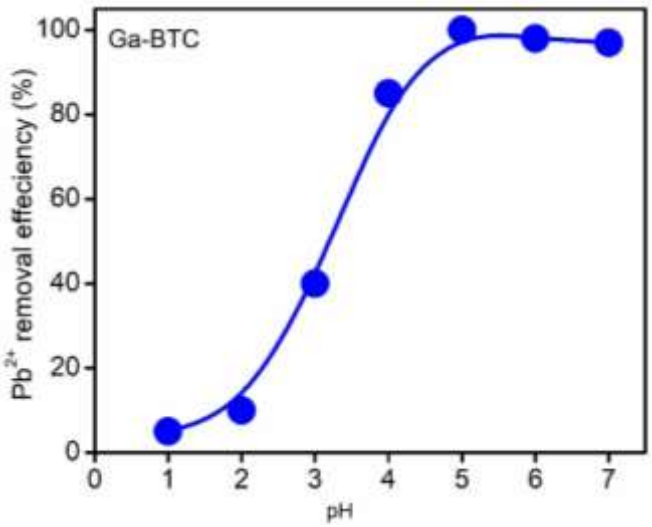

Figure 10: Effect of pH on the Pb^{2+} removal on Ga BTC MOF

Various heavy metal ion removal over Ga-BTC MOF (effect of nature of adsorbate)

Figure 11 represents the adsorption of various heavy metal ions taken in 100 ppm concentration, studied over Ga BTC MOF at room temperature. The selective adsorption of heavy metal ions was observed in the order of Pb^{2+} > Hg^{2+} > Cd^{2+} > Sb^{5+} > Sn^{4+} indicating that Ga BTC MOF exhibited higher efficiency and more selective towards lead ions as compared to other heavy metal ions. Pb^{2+}ions are border line Lewis acids while mercuric and cadmium ions are soft Lewis acids. Sb^{5+} and Sn^{4+}ions are known to be hard Lewis acids. The electrostatic interactions and chelation with organic linkers that are possible adsorption mechanistic routes for the removal of heavy metal ions over MOFs indicate that adsorption efficiency is based on the extent of interactions

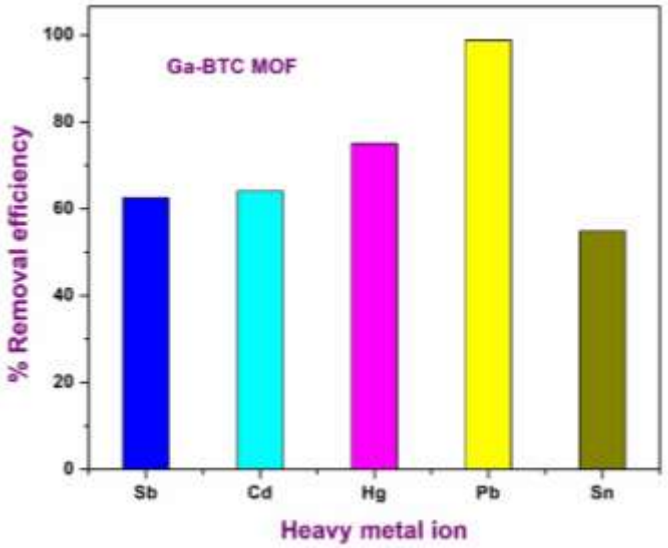

Figure 11: Heavy metal ion removal over Ga-BTC MOF

Pb(II), Cd(II) and Hg(II) removal over various BTC MOFs

The lead ion removal by adsorption was studied over 10 mg of the four different BTC MOFs prepared with a 20 ppm concentration of the lead nitrate solution. The study represented in figure 12 clearly indicates Ga BTC MOF to show higher efficiency in the selective adsorption of lead ion. This was followed by Zr BTC, Al BTC and least with Cu BTC. Thus, Ga BTC MOF was studied further for the adsorption of lead ion of higher concentration upto 400 ppm.

International Journal of Environmental Sciences
ISSN: 2229-7359
Vol. 11 No. 21s, 2025
https://www.theaspd.com/ijes.php

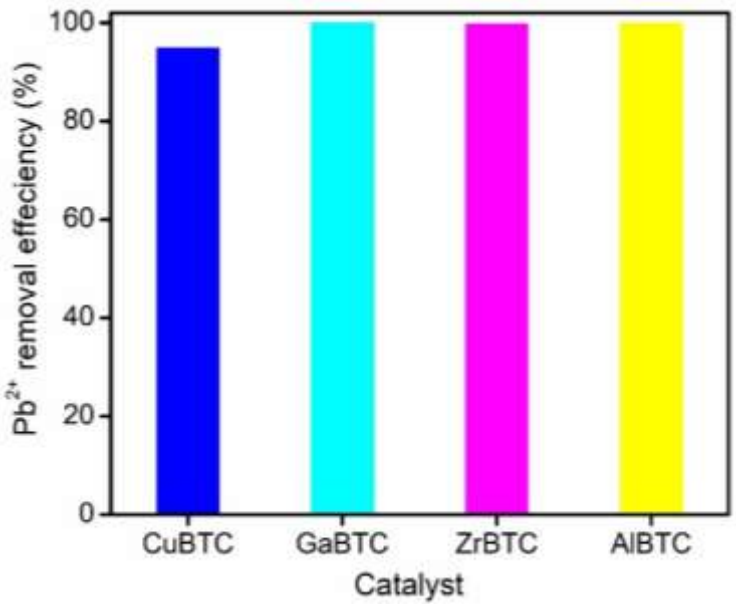

Figure 12: Pb^{2+} ion removal over various BTC MOFs

A similar study was carried out with 100 ppm aqueous solution of Cd^{2+} over 10 mg each of the four MOFs prepared (fig.12). The adsorption capacity or the removal efficiency of MOFs was in the order: Ga-BTC > Zr-BTC ≈ Cu BTC ≈ Al-BTC MOFs. A maximum of 64% removal efficiency was seen over Ga-BTC catalyst indicating selective adsorption of Cd^{2+} over Ga-BTC. Since, the organic linker is the same in all the MOFs, it implies that the interaction of cadmium ions with Ga^{3+} metal ion nodes is greater as compared to Zr^{4+}, $Al^{3+}$and Cu^{2+} metal nodes.

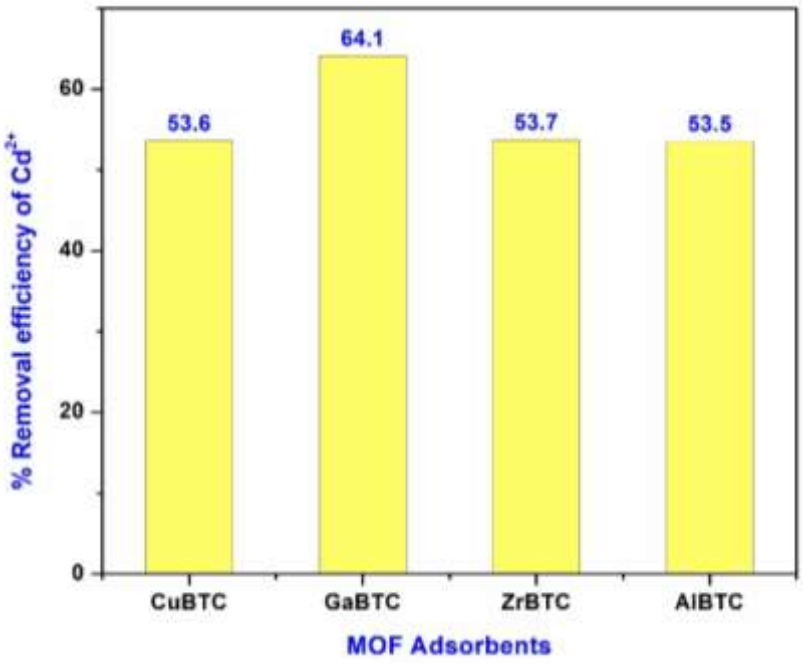

Figure 12: Cd^{2+} adsorption over various BTC MOFs

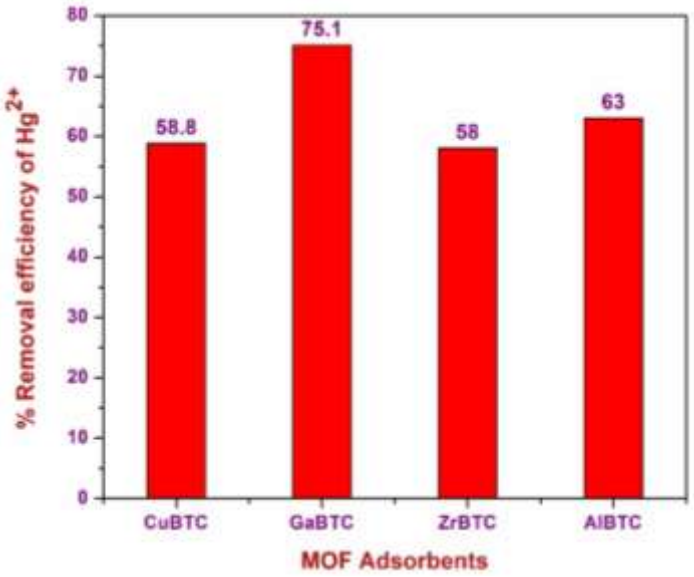

Figure 13: Hg^{2+} adsorption over various BTC MOFs

Figure 13 is a plot of removal efficiency of Hg^{2+} vs various BTC MOFs when a 100 ppm of aqueous solution of mercuric ions was subjected to adsorption over 10 mg of these MOFs. The highest adsorption capacity/removal efficiency of mercuric ions is exhibited by Ga-BTC MOF with a maximum removal efficiency of 75% followed by 63% removal efficiency by Al-BTC while the rest two MOFs showed nearly the same removal efficiency ~58%.

Effect of initial concentration and contact time on the removal efficiency of heavy metal ions over Ga-BTC MOF

A detailed study of adsorption of lead ions over Ga-BTC MOF which showed highest removal efficiency and selective adsorption towards lead ions was carried out varying the amounts of adsorbents, adsorbate and contact time (time interval for adsorption). The effect of concentration of lead ions on the adsorption efficiency of MOF is studied over Ga BTC MOF in the range of 20-400 ppm. A 100% removal efficiency was observed over Ga MOF upto 200 ppm while about 50% efficiency was seen with 400 ppm of Pb^{2+}solution. Table 2 below shows the variation of adsorption efficiency with the concentration of heavy metal ion solution over Ga BTC MOF. The effect of contact time as shown in fig. 14 for the adsorption of lead ions over Ga BTC MOF clearly indicates that maximum adsorption takes place within 60 min. of time and there after it is just the same and no further noticeable adsorption takes place. The same has been observed with the study of mercuric and cadmium ions adsorption over Ga-BTC and the rest of the other three BTC MOFs studied. Thus, all further studies with respect to variation in concentration of the adsorbates (heavy metal ions) and amounts of MOF taken were studied for 4-5 h adsorption and a constant % removal efficiency of the heavy metal ions is obtained.

Table 2: Variation in adsorption efficiency with concentration of heavy metal ions over Ga-BTC MOF

Pb^{+2}/ Cd^{+2}/ Hg^{+2} Concentration (ppm)	% Pb^{+2} Adsorption over Ga BTC	% Hg^{+2} Adsorption over Ga BTC	% Cd^{+2} Adsorption over Ga BTC
20	100	75.10	85.35
40	99.07	71.23	80.75
60	97.95	67.34	76.81
80	99.22	64.76	71.67
100	98.81	60.45	64.1
200	97.55	30.12	28.78

400	49.09	15.18	14.52

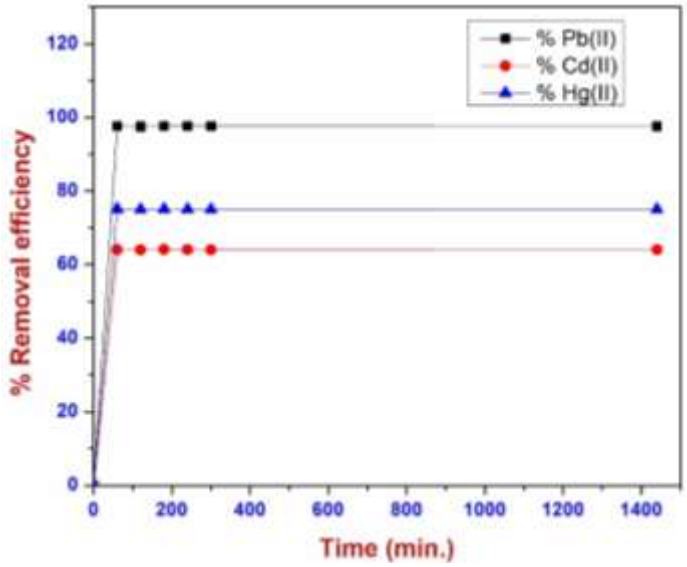

Figure 14: Effect of contact time on the adsorption efficiency of Pb^{2+}, Cd^{2+} & Hg^{2+} ions over Ga-BTC MOF

Adsorption Kinetics

The adsorption data of lead ions over Ga-BTC MOF is studied further by substituting the data into various kinetic models and plots to understand the behaviour this heavy metal ion adsorption over MOFs. Studies on adsorption of heavy metal ions over different adsorbents reported by various investigators mainly have taken the Langmuir-Hinshelwood model with both pseudo first order as well pseudo second order kinetic plots verified.

The linear form of the pseudo first order rate equation is given by

$$\ln(q_e - q_t) = \ln q_e - k_1 t$$

while the linear form of the pseudo second order rate equation is

$$\frac{t}{q_t} = \frac{1}{k_2 q_e^2} + \frac{1}{q_e} t$$

where q_e is the amount of heavy metal ions adsorbed at equilibrium in (mg g^{-1}); q_t is the amount heavy metal ions adsorbed at any time t in (mg g^{-1}); t is the time in min.; k_1 is the pseudo first order rate constant (min^{-1}) and k_2 is the pseudo second order rate constant (g $mg^{-1}min^{-1}$).

into the pseudo second order model. A plot of q_t vs initial concentration (fig. 15A) and the plot of $\frac{t}{q_t}$ vs t (fig. 15 B) clearly indicates a linear behaviour, shows a proper fit into the pseudo second order kinetic model with high correlation coefficient, $R^2 = 1$. A maximum adsorption of 976 mg g^{-1} of Pb^{2+}, 321 mg $g^{-1}$of Cd^{2+} and 375 mg $g^{-1}$of Hg^{2+}were obtained over Ga-BTC MOF. While 313 mg $g^{-1}$of $Sb^{5+}$and 261 mg $g^{-1}$of Sn^{4+}were adsorbed to a maximum extent on the same MOF.

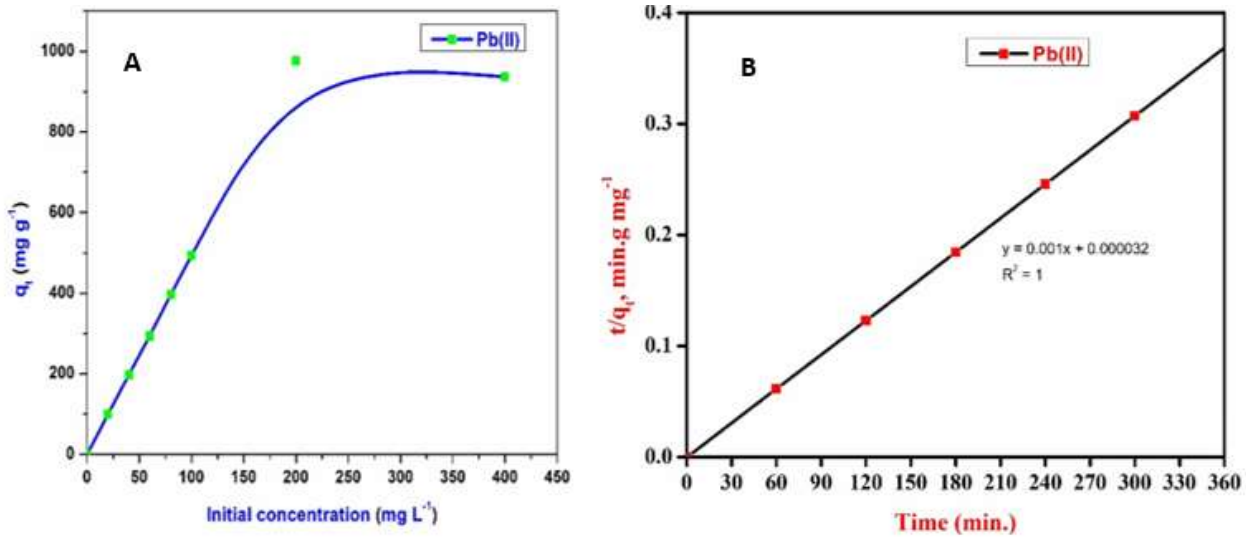

Figure 15: Kinetic plots of adsorption of Pb^{2+} over Ga-BTC MOFA) q_t vs initial conc. of Pb^{2+} B) t/q_t vs t

The table 3 below gives a comparison of adsorption of the heavy metal ions available in some of the reports on MOF materials with the MOFs studied in the present work.

Table 3: A comparison of adsorption efficiencies of various MOFs reported with the present study for heavy metal ion removal from aqueous matrix

MOF as adsorbent	Adsorption amount of Pb(II) in mg g^{-1}	Adsorption amount of Hg(II) in mg g^{-1}	Adsorption amount of Cd(II) in mg g^{-1}	Reference no.
Zn-thiazole (IUST-2)	1450	900	-	[25]
TMU-31	909	476	-	[24]
Zr-MOF	428.6	-	-	[26]
Zn-MOF	1097	33	-	[58]
Thiol-Cu-BTC	-	719	-	[31]
Fe_3O_4 - JUC-62	-	837.7	-	[29]
nFe_3O_4@MIL-88A(Fe)	-	-	693	[27]
UiO-66-NH_2	1795.3			[30]
UiO-66-NHC(S)	-	769	-	[30]
Fe_3O_4-Ga-BDC	220	-	-	[59]
TMU-5	-	-	634	[28]
Ga-BTC	976	375.2	320	Present work
Al-BTC	277.9	284.6	267.3	Present work
Zr-BTC	268.4	289.7	287.4	Present work
Cu-BTC	252.2	294	268	Present work

Reusability and Stability of MOFs

International Journal of Environmental Sciences
ISSN: 2229-7359
Vol. 11 No. 21s, 2025
https://www.theaspd.com/ijes.php

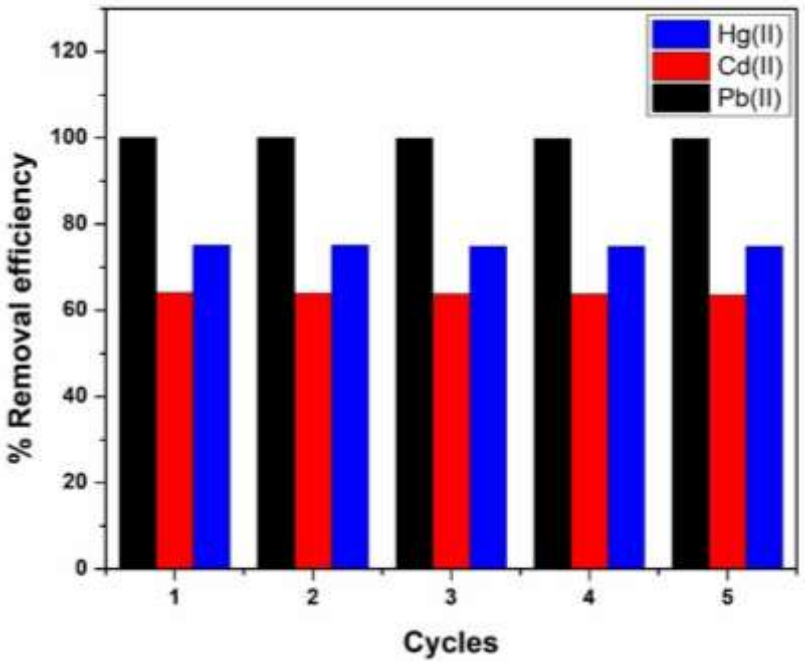

Figure 16: Reusability of Ga-BTC MOF for heavy metal ions removal

The reusability studies (fig.16) carried out over Ga BTC MOF for 100 ppm of the heavy metal ions viz., Pb^{2+}, Cd^{2+} and Hg^{2+} removal by adsorption over a time interval of 5 h clearly shows that Ga BTC MOF is efficient enough to remove the heavy metal ions even after 5 cycles of use. The MOF was centrifuged, filtered and washed with water after every batch of adsorption carried out. The MOF material after use was subjected to characterization by XRD and SEM-EDX to test the stability of the material and confirm the adsorbed metal ions presence on the MOFs respectively.

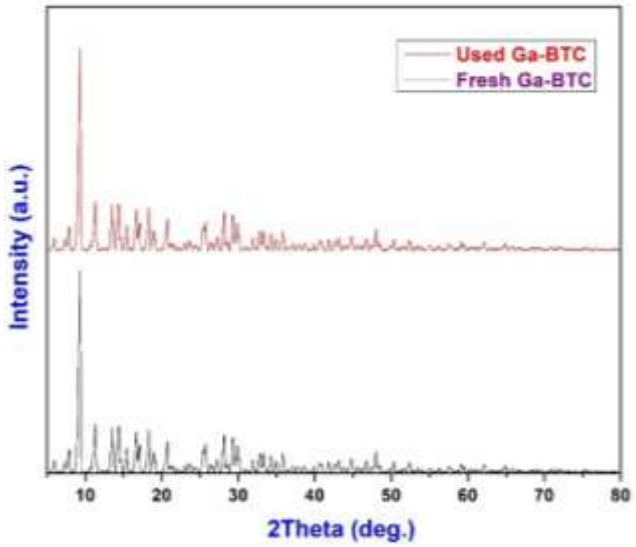

Figure 17: Fresh and Used Ga-BTC MOF XRD patterns

The figure 17 above clearly indicates the stability of Ga-BTC MOF from the used XRD pattern that is just the same as its fresh form without any structural changes. The SEM-EDX images (fig. 18) of the Ga-BTC after adsorption of Pb^{2+}, Hg^{2+} and Cd^{2+} which again not only establish the stability of the MOF but also confirm the presence of heavy metal ion on the surface of the Ga-BTC MOF.

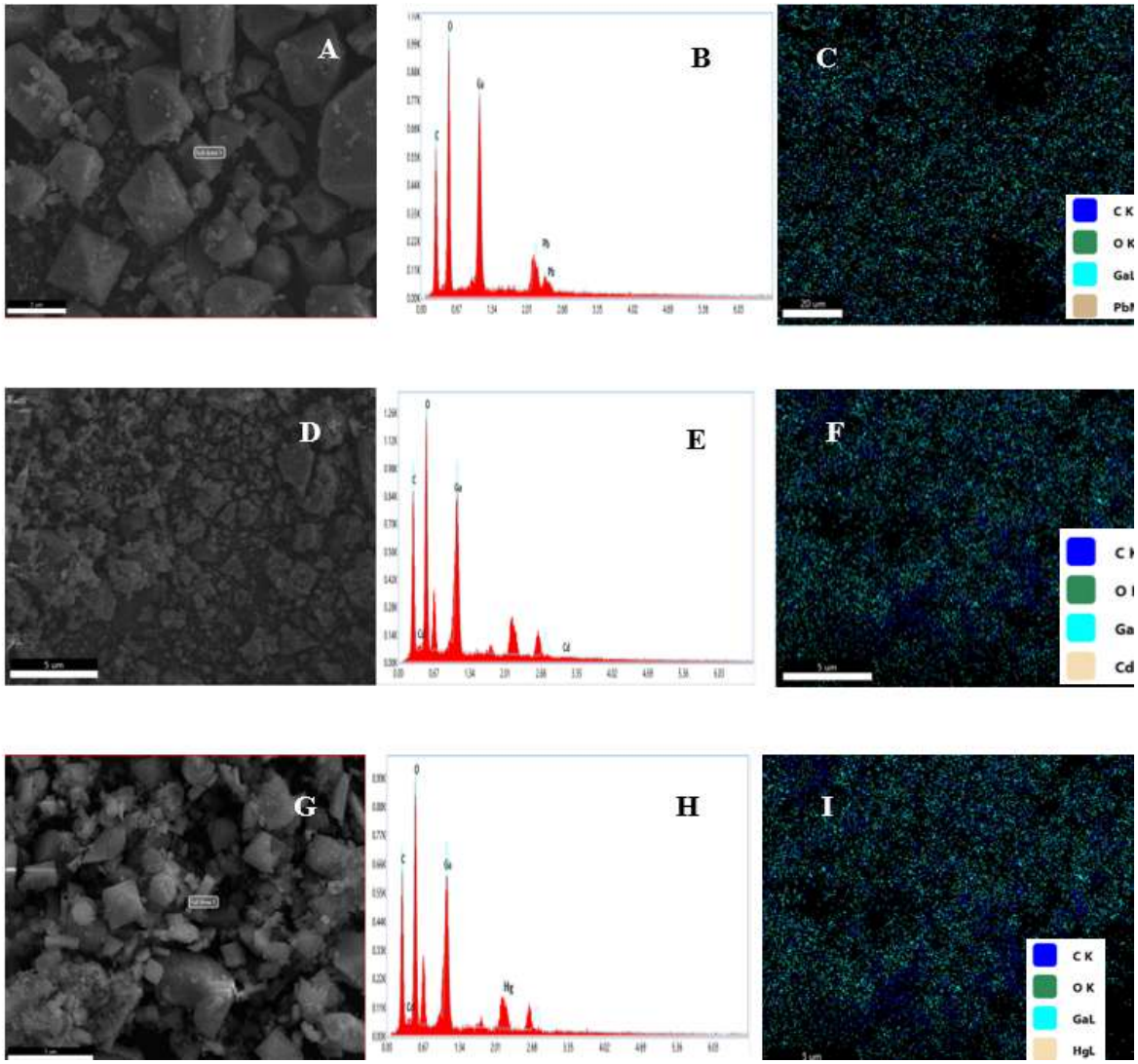

Figure 18: SEM-EDX & Elemental mapping of adsorption of A), B) & C) Pb^{2+}; D), E) & F) Cd^{2+}; G), H) & I) Hg^{2+}over Ga-BTC MOF

The adsorptive surface mechanism suggested involves various physical and chemical interactions responsible for the effective removal of toxic heavy metal ions where electrostatic interactions and chelation of these metal ions with MOFs in combination play major role [17] attributed to the higher efficiency of MOFs in the removal of heavy metal ions. Figure 19 below is a schematic representation of the plausible mechanism of adsorption of heavy metal ions over MOFs in the current study.

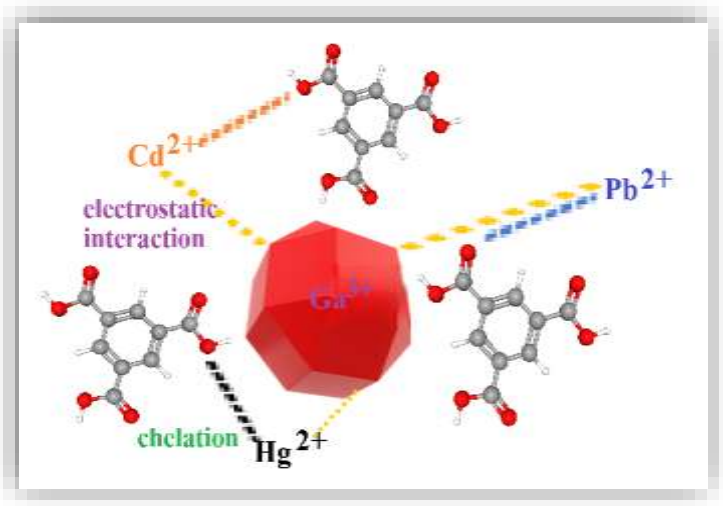

Figure 19: Plausible Surface mechanistic approaches for the adsorption of heavy metal ions over BTC MOFs

CONCLUSIONS

Four different BTC MOFs viz., Ga-BTC, Al-BTC, Zr-BTC and Cu-BTC were prepared by solvo hydrothermal method which were found to be highly crystalline, microporous and high surface area materials. They were found to be stable upto around 350 ^{o}C as noticed from thermogravimetric analysis. The FT-IR and Raman spectra showed characteristic vibrational modes of carboxylate groups and the M-O-M bonds. The MOFs displayed cubo-octahedral/polyhedron morphologies of uniform size. The MOFs were selective in the removal of heavy metal ions, among which Ga-BTC MOF was found to be highly potential in the removal of metal ions which is more selective in the removal of Pb(II) ions. The removal capacity of Pb(II), Cd(II) and Hg(II) over the four MOFs studied was in the order: Ga-BTC > Zr-MOF > Al-MOF > Cu-MOF. The variable conditions studied in the adsorption of lead ions over Ga-BTC indicated the process to follow a pseudo second order kinetics with the plot fitting quiet well into this model with a very high correlation coefficient of R^2 = 1. The maximum removal capacity of Pb^{2+} ions over Ga-BTC MOF was found to be 976 mg g^{-1}. The removal capacity of heavy metal ions over Ga-BTC followed the order: $Pb^{2+} > Hg^{2+} > Cd^{2+} > Sn^{4+} > Sb^{5+}$. MOFs were found to exhibit high adsorption capacities in the removal of heavy metal ions through both physical and chemical interactions mainly through coordination with the metal nodes via electrostatic interactions and chelation possible with the organic linkers on the large surface and porous structure of the MOFs that enhance the removal efficiencies of the heavy metal ions. Ga-BTC MOF was found to be reusable with its structure intact even after 5 cycles of use without any loss in its adsorption capacity in the removal of heavy metal ions more specifically lead ions from aqueous matrix. The Ga-BTC MOF is recognized as a highly potential adsorbent in the removal of toxic heavy metal ions from aqueous solutions even without any N or S containing ligands or magnetic components. Thus, Ga-BTC MOF may be suggested as a potential adsorbent for the removal of toxic metal ions from effluents involving high concentrations of toxic heavy metal ions.

CONFLICT OF INTEREST

Authors declare no conflict of interest.

ACKNOWLEDGMENTS

The authors are thankful to Dr. A. Venugopal, Chief Scientist, CSIR-IICT, Hyderabad for the help rendered with respect to some of the characterization of the MOFs. Acknowledgements are due to the Central Facility for Research & Development, Osmania University, Hyderabad for the XPS analysis.

REFERENCES :

[1] Barakat M A, New Trends in Removing Heavy Metals from Industrial Wastewater, 2011, Arab J Chemistry, 4, 361-

377.

[2] Kobielska P A, Howarth A J, Farha OK, Nayak S, Metal–organic frameworks for heavy metal removal from water, 2018, Coord Chem Rev 358, 92-107.

[3] Chen D, Shen W., Wu S., Chen C., Luo X., Guo L, Ion exchange induced removal of Pb(II) by MOF-derived magnetic inorganic sorbents. 2016, Nanoscale, 8, 7172–7179.

[4] Zahir F, Rizwi S J, Haq S K and Khan R H, Low dose mercury toxicity and human health, 2005, Environ Toxicol Pharmacol, 20, 351–360.

[5] Hatzidaki E, Tzanakakis G N and Tsatsakis A M, Lead toxicity update. A brief review, 2005, Med Sci Monit, 11(10), 329–336.

[6] Haider F U, Liqun C, Coulter J A, Cheema S A, Wu J, Zhang R, Wenjun M and Farooq M, Cadmium toxicity in plants: Impacts and remediation strategies, 2021, Ecotoxicol Environ Saf, 211, 111887.

[7] Karababa H, Atasoy M, Yildiz D, Kula I and Tuzen M, Development of a Sensitive Method for Cadmium Determination in Fish Tissue and Drinking Water Samples by FAAS Using SQT In Situ Atom Trapping, 2023, ACS Omega, 8, 7063–7069.

[8] Ledezma C Z-, Bolagay D N-, Figueroa F, Ledezma E Z-, Ni M, Alexis F and Guerrero V H, Heavy metal water pollution: A fresh look about hazards, novel and conventional remediation methods, 2021, Environ Technol Innovation, 22, 101504.

[9] Imran Ali, New Generation Adsorbents for Water Treatment, 2012, Chemical Reviews 112 (10), 5073-5091.

[10] Xu S, Lv Y, Zeng X, Cao D, ZIF-derived nitrogen-doped porous carbons as highly efficient adsorbents for removal of organic compounds from wastewater, 2017, Chem Eng J, 323, 502–511.

[11] Sublet R, Simonnot M -O, Boireau A, Sardin M, Selection of an adsorbent for lead removal from drinking water by a point-of-use treatment device, 2003, Water Res 37(20), 4904–4912.

[12] Edokpayi JN, Odiyo JO, Popoola EO, Alayande OS, Msagati TAM, Synthesis and Characterization of Biopolymeric Chitosan Derived from Land Snail Shells and Its Potential for Pb^{2+} Removal from Aqueous Solution. 2015, Materials (Basel). 10;8(12):8630-8640.

[13] Sudik A C, Antek P C, Foy G W, O'Keeffe M and Yaghi O M, A metal-organic framework with a hierarchical system of pores and tetrahedral building blocks, 2006, Angew. Chem Int Ed Engl, 45, 2528-2533.

[14] Chen B L, Ockwig N W, Millard A R, Contreras D S and Yaghi O M, High H_2 adsorption in a microporous metal-organic framework with open metal sites, 2005, Angew Chem Int Ed Engl, 44, 4745-4749.

[15] Kim J, Lin B, Reineke T M, Li H, Eddaoudi M, O'Keeffe M and Yaghi O M, Rod packings and metal-organic frameworks constructed from rod-shaped secondary building units, 2001, J Am Chem Soc, 123, 8239-8247.

[16] Rowsell, J. L. C.; Yaghi, O. M, Metal–organic frameworks: a new class of porous materials, Micropor. Mesopor. Mater., 2004, 73, 3-14.

[17] Essalmi S, Lotfi S, BaQais A, Saadi M, Arab M and Ahsaine H A, Design and application of metal organic frameworks for heavy metals adsorption in water: a review, 2024, RSC Adv, 14, 9365-9390.

[18] Gao M, Liu G, Gao Y, Chen G, Huang X, Xu X, Wang J, Yang X and Xu D, Recent advances in metal-organic frameworks/membranes for adsorption and removal of metal ions, 2021, Trends in Analytical Chemistry 137, 116226.

[19] Li X, Ma W, Li H, Zhang Q & Liu H, Sulfur-functionalized metal-organic frameworks: Synthesis and applications as advanced adsorbents, 2020, Coord Chem Rev 408, 213191.

[20] Awad S F, Bakry A M, Ibrahim A A, Lin A & El-Shall M S, Thiol-and amine-incorporated UIO-66-NH_2 as an efficient adsorbent for the removal of Mercury (II) and phosphate ions from aqueous solutions, 2021, Ind Eng Chem Res 60, 12675–12688.

[21] Paz R, Viltres H, Gupta N K, Galarza A R- and Leyva C, Magnetic MOF-808 as a novel adsorbent for toxic metal removal from aqueous solutions, 2022, Environ Sci Adv, 1, 182–191.

[22] Zhang Y, Liu L, Yu D, Liu J, Zhao L, Liu J and Liu S, Preparation of Magnetic MIL-68(Ga) Metal–Organic Framework and Heavy Metal Ion Removal Application. 2022, Molecules, 27, 3443.

[23] Guo H, Wang M, Liu J, Zhu S and Liu C, Facile synthesis of nanoscale high porosity IR-MOFs for low-k dielectrics thin films, 2016, Microporous and Mesoporous Materials, 221, 40-47.

[24] Hakimifar A and Morsali A, Urea-Based Metal-Organic Frameworks as High and Fast Adsorbent for $Hg^{2+}$and Pb^{2+} Removal from Water, 2018, Inorg Chem 58, 180–187.

[25] Hosseini A K & Tadjarodi A, Novel Zn metal–organic framework with the thiazole sites for fast and efficient removal of heavy metal ions from water, 2023, Scientific Reports, 13, 11430.

[26] Wang C., Xiong C., He Y., Yang C., Li X., Zheng J., Wang S. Facile preparation of magnetic Zr-MOF for adsorption

of Pb(II) and Cr(VI) from water: Adsorption characteristics and mechanisms, 2021, Chemical Engineering Journal, 415, 128923.

[27] Mahmoud M E, Amira M F, Seleim S M and Mohamed A K, Amino-decorated magnetic metal-organic framework as a potential novel platform for selective removal of chromium (Vl), cadmium (II) and lead (II), 2020, J Hazar Mater, 381, 120979.

[28] Ul Mehdi S and Aravamudan K, Adsorption of cadmium ions on silica coated metal organic framework. 2022, Mater Today Proc, 61, 487–497.

[29] Wu Y., Xu G., Wei F., Song , Tang T., Wang X., Hu Q. Determination of Hg (II) in tea and mushroom samples based on metal-organic frameworks as solid phase extraction sorbents, 2016, Microporous and Mesoporous Materials, 235, 204-210.

[30] Saleem H, Rafique U and Davies R P, Investigations on post-synthetically modified UiO-66-NH_2 for the adsorptive removal of heavy metal ions from aqueous solution, 2016, Microporous and Mesoporous Materials, 221, 238-244.

[31] Ke F, Qiu L G, Yuan Y P, Peng F M, Jiang X, Xie A J, Shen Y H and Zhu J F, Thiol-functionalization of metal-organic framework by a facile coordination-based post synthetic strategy and enhanced removal of Hg^{2+} from water, 2011, J Hazard Mater, 196, 36-43.

[32] Venu B, Shirisha V, Vishali B, Naresh G, Kishore R, Sreedhar I and Venugopal A, A Cu-BTC metal–organic framework (MOF) as an efficient heterogeneous catalyst for the aerobic oxidative synthesis of imines from primary amines under solvent free conditions, 2020, New J Chem, 44, 5972-5979.

[33] Garibay S J and Cohen S M, Isoreticular synthesis and modification of frameworks with the UiO-66 topology, 2010, Chem Commun 46 (41), 7700-7702.

[34] Loiseau T, Lecroq L, Volkringer C, Marrot J, Férey G, Haouas Md, Taulelle F, Bourrelly S, Llewellyn P L and Latroche M, MIL-96, a Porous Aluminum Trimesate 3D Structure Constructed from a Hexagonal Network of 18-Membered Rings and μ_3-Oxo-Centered Trinuclear Units, Journal of the American Chemical Society 2006 128 (31), 10223-10230.

[35] Yang L, Ruess G L and Carre M A, Cu, Al and Ga based metal organic framework catalysts for the decarboxylation of oleic acid, 2015, Catal Sci Technol, 5, 2777-2782.

[36] The Kagomé Topology of the Gallium and Indium Metal-Organic Framework Types with a MIL-68 Structure: Synthesis, XRD, Solid-State NMR Characterizations, and Hydrogen Adsorption, Volkringer C, Meddouri Md, Loiseau T, Guillou N, Marrot J, Férey G, Haouas Md, Taulelle F, Audebrand N, and Latroche M, 2008, Inorg Chem, 47, 24, 11892–11901.

[37] Chen Y, Mu X, Lester E and Wu T, High efficiency synthesis of HKUST-1 under mild conditions with high BET surface area and CO_2 uptake capacity, 2018, Prog Nat Sci Mater Int, 28, 584–589.

[38] Esfahani HJ, Shahhosseini S & Ghaemi A, Improved structure of Zr-BTC metal organic framework using NH_2 to enhance CO_2 adsorption performance, 2023, Sci Rep 13, 17700.

[39] Loiseau T, Serre C, Huguenard C, Fink G, Taulelle F, Henry M, Bataille T and Férey G, A Rationale for the Large Breathing of the Porous Aluminum Terephthalate (MIL-53) Upon Hydration, 2004, Chem Eng J, 10, 1373-1382.

[40] Gurmessa B K, Taddess A M and Teju E, UiO-66 (Zr-MOF): Synthesis, characterization, and Application for the Removal of Malathion and 2, 4-D from Aqueous Solution, 2023, Environ Pollu Bioavail, 35(1), 2222910.

[41] Lin Y, Kong C and Chen L, Facile Synthesis of Aluminum-Based Metal–Organic Frameworks with Different Morphologies and Structures through an OH(−)-Assisted Method 2013, Chem Asian J, 8,1873–1878.

[42] Schlichte K, Kratzke T, and Kaskel S, Improved synthesis, thermal stability and catalytic properties of the metal-organic framework compound Cu3(BTC)2, 2004, Micro and Meso Mater, 73, 81–88.

[43] Abid H R, Rada Z H, Shang J and Wang S, Physicochemical characterization of metal organic framework materials: A mini review, 2016, Polyhedron, 120, 103-111.

[44] Xu J, Liu J, Li Z, Wang X, Xu Y, Chen S and Wang Z, Optimized synthesis of Zr(iv) metal organic frameworks (MOFs-808) for efficient hydrogen storage, 2019, New J. Chem., 43, 4092-4099.

[45] Ghafuri H, Ganjali F and Hanifehnejad P, Cu-BTC MOF as a Novel and Efficient Catalyst for the Synthesis of 1,8-Dioxo-octa-hydro Xanthene, 2021, Chem Proc, 3, 2.

[46] Moloto W, Mbule P, Nxumalo E and Ntsendwana B, Stabilizing effects of zinc(II)-benzene-1,3,5-tricarboxylate metal organic frameworks on the performance of TiO2 photoanodes for use in dye-sensitized solar cells, 2021, J Photochem Photobiol A, 407, 113063.

[47] Zou X, Zhu G, Hewitt F and Qiu S S, Synthesis of a metal–organic framework film by direct conversion technique for VOCs sensing, 2009, J Chem Soc Dalt Trans, 16, 3009-3013.

[48] Guo R, Deng Y, Jia Y, Shi C, Zhang W, Zhou Y and Hou X, Gallium ions induced in-situ MOF-derived hierarchical

porous Co_3O_4 for ultra-high acetone response, 2024, Sensors and Actuators: B. Chemical, 399, 134832.

[49] Dong Z, Mi Z, Shi W, Jiang H, Zheng Y and Yanga K, High pressure effects on hydrate Cu-BTC investigated by vibrational spectroscopy and synchrotron X-ray diffraction, 2017, RSC Adv, 7, 55504–55512.

[50] Arjmand F & Ranjbar Z R, Impact of copper and cobalt-based metal-organic framework materials on the performance and stability of hole-transfer layer (HTL)-free perovskite solar cells and carbon-based, 2024, Sci. Reports, 14, 12843.

[51] Gurushantha, K.; Anantharaju, K.S.; Renuka, L.; Sharma, S.C.; Nagaswarupa, H.P.; Prashantha, S.C.; Vidya, Y.S.; Nagabhushana, H.; RSC Adv., 2017, 7 (12) 12690-12703.

[52] Wang X, Zhu H, Sun T, Liu Y, Han T, Lu J, Dai H and Zhai L, Synthesis and Study of an Efficient Metal-Organic Framework Adsorbent (MIL-96(Al)) for Fluoride Removal from Water, 2019, J Nanomaterials, 3128179.

[53] Wang K, Ye W, Yin W, Chai W, Rui Y and Tang B, One-step synthesis of MOF-derived Ga/Ga_2O_3@C dodecahedra as an anode material for high-performance lithium-ion batteries, 2019, Dalton Trans, 48, 12386-12390.

[54] Sandra J, Munmun G and Anitha V, Tweaking the electrocatalytic ability of Cu-MOF by the inclusion of PTA: a selective electrochemical sensor for resorcinol, 2024, Mater. Adv, 5, 3812-3823.

[55] Tang J, Zhang S, Chen X, Zhang L, Du L and Zhao Q, Highly Efficient Catalytic Reduction of Nitrobenzene Using Cu@C Based on a Novel Cu–MOF Precursor, 2023, Catalysts, 13, 956

[56] Wang K, Gu J, and Yin N, Efficient removal of Pb (II) and Cd (II) using NH_2-functionalized Zr-MOFs via rapid microwave-promoted synthesis, 2017, Ind Eng Chem Re, 56, 1880—1887.

[57] Jadoun S, Fuentes J P, Urbano B F and Y´a˜nez J, Solar-Assisted Synthesis of Poly(o-phenylenediamine)@Zinc Oxide Composites for Photocatalytic Cu(II) Ion Removal, 2023, J Wat Proc Eng 53, 103663.

[58] Huang Z, Zhao M, Wang C, Wang S, Dai L, Zhang L, Preparation of a Novel Zn(II)-Imidazole Framework as an Efficient and Regenerative Adsorbent for Pb, Hg, and As Ion Removal From Water, 2020, ACS Appl Mater Interfaces, 12, 41294–41302.

[59] Zhang Y, Liu L, Yu D, Liu J, Zhao L, Liu J and Liu S, Preparation of Magnetic MIL-68(Ga) Metal–Organic Framework and Heavy Metal Ion Removal Application, 2022, Molecules, 27, 3443.